

Host Galaxy Contribution to the Colours of ‘Red’ Quasars

F. J. Masci,^{1*} R. L. Webster^{1†} and P. J. Francis^{2‡}

¹*School of Physics, University of Melbourne,
Parkville, Victoria 3052, Australia*

²*Department of Physics and Theoretical Physics, Faculty of Science,
Australian National University, Canberra, ACT 0200, Australia*

Zeroth Draft

ABSTRACT

We describe an algorithm that measures self-consistently the relative galaxy contribution in a sample of radio-quasars from their optical spectra alone. This is based on a spectral fitting method which uses the size of the characteristic 4000Å feature of elliptical galaxy SEDs. We apply this method to the Parkes Half-Jansky Flat Spectrum sample of Drinkwater et al. (1997) to determine whether emission from the host galaxy can significantly contribute to the very red optical-to-near-infrared colours observed. We find that at around 2σ confidence, most of the reddening in unresolved (mostly quasar-like) sources is unlikely to be due to contamination by a red stellar component.

Key words: galaxies: colours – methods: analytical – quasars: general

1 INTRODUCTION

The recent discovery of large numbers of radio-selected quasars with very red optical-to-near-infrared colours suggests that existing quasar surveys may be severely incomplete. Based on a high identification rate in the optical and near-infrared, Webster et al. (1995) found a broad range of colours with $2 < B - K < 10$ for flat-spectrum radio quasars in a subsample of the Parkes 2.7GHz survey (Drinkwater et al. 1997; hereafter ‘Parkes quasars’). For comparison, quasars selected by standard optical techniques show a small scatter around $B - K \sim 2.5$. Two theories have been proposed to explain the large scatter: first, Webster et al. (1995) interpreted this in terms of extinction by line-of-sight dust (see also Masci 1997), and second, Serjeant & Rawlings (1996) suggested that this was due to intrinsically red optical/infrared synchrotron radiation associated with the radio emission. This paper explores a third possibility: that the red colours are due to contamination by starlight from the host galaxies.

In a recent near-infrared imaging study of a sample of radio-quasars selected from the low-frequency (408MHz) catalog, Benn et al. (1998) found that sources with red $B - K$ colours to $z \sim 2$ could be explained by an excess of host galaxy light in K . Most of the images appeared non-stellar (or resolved) suggesting that indeed starlight was responsible for the redness in $B - K$ colour. It is important to note

however that all these sources were associated with extended radio galaxies of which a majority are of the steep-spectrum type, a common feature of low-frequency selected samples. A large fraction are also often associated with luminous giant ellipticals. In view of the simple orientation-based unified model for radio-loud AGN, it is possible that galaxy light is more easily detected in these sources due to anisotropic obscuration and/or unbeamed emission of the central AGN. The radio-quasars explored in this paper are all of the flat-spectrum type selected at moderately high frequency. Thus, they are not expected to exhibit similar properties in the near-infrared.

The $B - K$ colours of normal radio galaxies are known to be quite red, exhibiting a similar dispersion to those observed in the Parkes sample. These sources are often associated with giant ellipticals and their colours appear to be uniformly distributed over the range $3 \lesssim B - K \lesssim 7$ for redshifts $z \lesssim 2$ (McCarthy 1993 and references therein). It is possible that the host galaxies of Parkes quasars also exhibit similar properties. To determine the importance of host galaxy light in Parkes quasars, we need to quantify its contribution throughout the optical to near-IR wavelength region.

Determining the host galaxy properties of radio-quasars and BL-Lac-type sources are crucial for studies of AGN evolution and testing unified schemes. A significant number of BL-Lacs and other core-dominated radio loud AGN are surrounded by nebulosities whose optical spectra are very similar to those of giant ellipticals (eg. Miller, French & Hawley 1978; Ulrich 1988; Taylor et al. 1996). A majority of these host galaxies have been detected in sources at relatively low redshifts, $z \lesssim 0.1$, where the galaxy flux is easily detected. Since most quasars are at high redshifts,

* Email: fmasci@physics.unimelb.edu.au

† Email: rwebster@physics.unimelb.edu.au

‡ Email: pfrancis@mso.anu.edu.au

host galaxy detections have been difficult due to contamination by their strong nuclear emission. Recent high resolution imaging using HST has revealed that a majority of high redshift quasars also reside in giant ellipticals (Hutchings & Morris 1995; Bahcall et al. 1995).

The optical spectral energy distributions (SEDs) of ellipticals are all similar in shape. At $\lambda \gtrsim 3000\text{\AA}$, they rise steeply up to $\sim 4000\text{\AA}$ where a sharp step-like cutoff is observed. This cutoff is often referred to as the “4000 Angstrom break” and is caused by the dearth of hot and young, usually O and B-type stars with time, whose spectra mostly dominate at wavelengths from $\approx 4000\text{\AA}$ into the UV. For $\lambda \lesssim 4000\text{\AA}$, the existence of a multiplet of heavy metal absorption lines arising from stellar atmospheres, results in a steepening of the break. The presence of this feature thus provides a signature for determining whether an underlying elliptical host is contributing to the total light.

In this paper, we describe a new unbiased method that uses the size of this characteristic break in the optical spectra of Parkes quasars to quantify the host galaxy contribution. We use this method to investigate whether the host galaxies of Parkes quasars can significantly contribute to the optical and near-IR continua and hence cause the spread in $B - K$ colours observed.

This paper is organised as follows: In section 2, we outline our method used to quantify the host galaxy contribution. A discussion of the spectral data and assumed input parameters is given in section 3. Results are presented in section 4. Implications for AGN unified schemes are explored in section 5 and results discussed in section 6. All results are summarised in section 7.

2 OUTLINE OF METHOD

The galaxy contribution can be estimated using an algorithm that determines the relative strength of the characteristic 4000\AA break in the optical spectra of Parkes sources in an unbiased way. No other feature in a generic quasar spectrum will mimic this feature. In this section, we describe this algorithm.

2.1 Assumptions

There are two important assumptions that will be required by our algorithm. First, we assume that the spectral shape defining an underlying quasar optical continuum is ‘smooth’ and contains no breaks. This is justified by our current knowledge of quasar optical spectra. Our choice for this shape is somewhat arbitrary, and will be further discussed in section 2.2.

Second, we need to assume the input galaxy spectrum which defines the shape of the 4000\AA break to be used in our analysis. We have formed a composite optical spectrum of 18 Parkes sources all of which appear ‘spatially extended’ in B_J . This composite is shown as the solid curve in Fig. 1 and clearly shows the characteristic 4000\AA break. Superimposed (dashed) is an elliptical galaxy SED predicted from the stellar population synthesis models of Bruzual & Charlot (1993). This model is for a galaxy of age 8Gyr, and assumes a 1Gyr burst described by a Salpeter initial mass function with no star formation thereafter. In fact, any ‘old

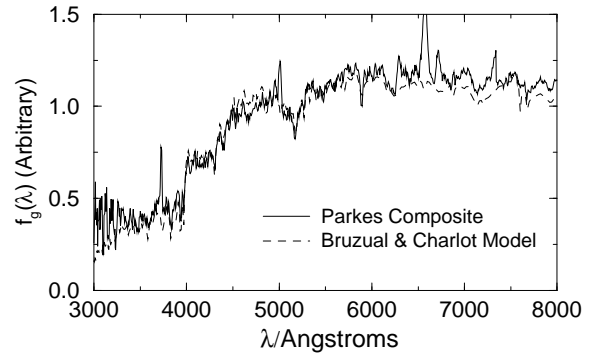


Figure 1. Composite optical spectrum of 18 Parkes sources which appear spatially extended in B_J (solid curve), and a model spectrum for an ‘old’ elliptical SED from Bruzual & Charlot (1993) (dashed curve).

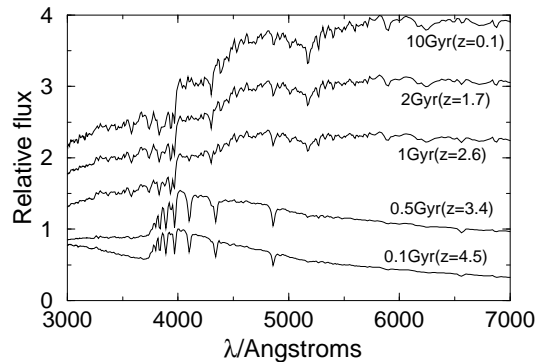


Figure 2. Spectral evolution of the 1Gyr burst model of Bruzual & Charlot (1993). The age in Gyr and the approximate corresponding redshift for a formation epoch $z_f = 5$ with $(q_0, h_{50}) = (0.5, 1)$ is shown beside each spectrum.

aged’ model with long completed star formation will in general be similar. Models assuming ‘long lived’ constant star formation rates lead to considerably bluer optical-UV continua, characteristic of those observed in spirals. The composite and model in Fig. 1 are in excellent agreement, except for the emission lines arising from ISM gas in the composite. In our analysis, we shall assume that this model represents the underlying elliptical SED in each of our Parkes sources.

For sources with redshifts $z \gtrsim 1$, the 4000\AA break is redshifted out of the wavelength range available in the spectra of Parkes quasars (see section 3.1) and thus, cannot be used in our algorithm. We are therefore restricted to $z < 1$. For simplicity, we assume that the general shape of our model elliptical SED is independent of redshift to $z \sim 1$. The colours of radio galaxies observed to $z \sim 3$ are consistent with formation redshifts $4 \lesssim z_f \lesssim 20$ (Spinrad & Djorgovski 1987; Dunlop et al. 1989). These formation redshifts are also suggested by

models of galaxy formation in the CDM scenario (eg. White & Frenk 1991). The spectral synthesis models predict that the general form of an elliptical SED shown in Fig. 1 can be immediately established following an almost instantaneous ($\sim 1\text{Gyr}$) burst of star formation. Adopting the 1Gyr burst model of Bruzual & Charlot (1993) (updated 1995 models), we show in Fig. 2 the spectral evolution as a function of age since the initial starburst. Also shown beside each age is the approximate redshift for a formation epoch of $z_f = 5$. Initially, the 4000\AA break region is diluted by starburst activity. After a few gigayears, the stellar population evolves passively, maintaining an almost uniform SED shape (see Bruzual & Charlot 1993). For formation epochs $z \gtrsim 5$, it is apparent that the generic elliptical SED shape of Fig. 1 is easily established by $z \sim 1$.

2.2 The Algorithm

In general, the total flux at a given wavelength observed in a Parkes source, $f_T(\lambda)$, can be modelled as the sum of light contributed by the central quasar or AGN, $f_q(\lambda)$, and any underlying host galaxy $f_g(\lambda)$ (eg. Fig. 1). We write the relationship between these quantities as:

$$f_q(\lambda) = f_T(\lambda) - c f_g(\lambda), \quad (1)$$

where c is a scaling factor giving an arbitrary measure of the amount of galaxy light we wish to determine for a particular source.

Given $f_T(\lambda)$ for a particular source and an arbitrary galaxy spectrum $f_g(\lambda)$ (Fig. 1), our aim is to determine the value of c such that $f_q(\lambda)$ looks something like a quasar spectrum. From our knowledge of quasar optical spectra, an obvious choice is to require that $f_q(\lambda)$ be “smooth” and contain no breaks. Thus, the basis of this algorithm involves subtracting an arbitrary amount of galaxy flux, $c f_g(\lambda)$ from $f_T(\lambda)$ such that the resulting spectrum $f_q(\lambda)$ appears smooth (see below). When this is achieved, the fraction of total light at a given wavelength contributed by the host galaxy can be estimated by normalising:

$$F_{gal}(\lambda) = \frac{c f_g(\lambda)}{f_T(\lambda)}. \quad (2)$$

In order to implement the above algorithm, we need to define an acceptable form for the shape of the quasar spectrum $f_q(\lambda)$. Our only requirement is that this spectrum be smooth and hence our choice is somewhat arbitrary. We choose $f_q(\lambda)$ to be a power-law, parameterised by:

$$f_q(\lambda) = f_q(\lambda_{max}) \left(\frac{\lambda}{\lambda_{max}} \right)^\alpha, \quad (3)$$

where the slope α is determined between two fixed wavelengths, λ_{min} and λ_{max} (see below):

$$\alpha = \frac{\ln [f_q(\lambda_{min})/f_q(\lambda_{max})]}{\ln [\lambda_{min}/\lambda_{max}]}. \quad (4)$$

Using Eqn. 1, the fluxes defined in Eqn. 4 can be written:

$$f_q(\lambda_{min}) = f_T(\lambda_{min}) - c f_g(\lambda_{min}) \quad (5)$$

$$f_q(\lambda_{max}) = f_T(\lambda_{max}) - c f_g(\lambda_{max}).$$

For a discussion on how the wavelengths λ_{min} and λ_{max} are chosen and the fluxes in Eqn. 5 measured, see section 3.1.

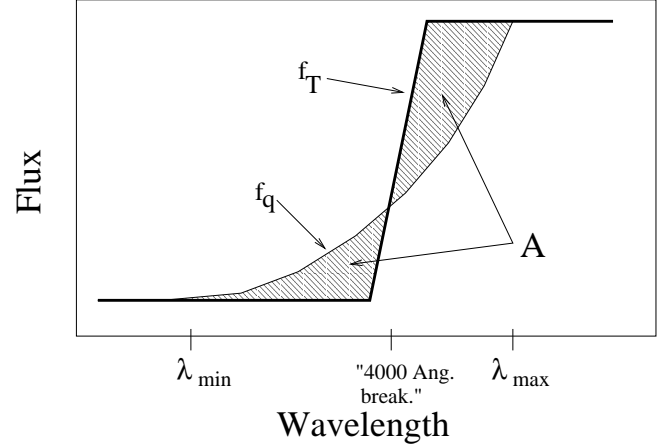


Figure 3. Definition of our “figure of merit” A . For a particular source spectrum $f_T(\lambda)$ (whose 4000\AA break region is shown exaggerated), we subtract an amount of galaxy flux, $f_g(\lambda)$ (Fig. 1) until A is a minimum and a smooth power-law $f_q(\lambda)$ results.

The validity of our assumption of a single power-law for $f_q(\lambda)$ is discussed in section 6.

To apply this algorithm in a self consistent way to each of our optical spectra, we need to define a figure of merit indicating the point at which the maximum amount of galaxy spectrum has been subtracted and a “smooth” quasar spectrum (ie. a power-law) is achieved. Let us first consider the rest frame optical spectrum of a source, $f_T(\lambda)$, suspected of containing a 4000\AA break. This is illustrated in Fig. 3. Furthermore, let us consider a “smooth” power-law (ie. the underlying quasar spectrum $f_q(\lambda)$) between two wavelengths λ_{min} and λ_{max} on either side of the 4000\AA break region as shown. We define our figure of merit as representing the area A of the shaded region in Fig. 3. As certain amounts of galaxy spectrum, $c f_g(\lambda)$ (where $f_g(\lambda)$ is given by Fig. 1) are gradually subtracted from $f_T(\lambda)$, A will decrease and becomes a minimum when the break disappears. We can thus determine the value of c when this occurs, allowing us to estimate the fractional galaxy contribution from Eqn. 2.

For a given amount of subtracted galaxy flux, $c f_g(\lambda)$, we can write A in terms of c from Eqn. 1 as follows:

$$A = \int_{\lambda_{min}}^{\lambda_{max}} |f_q(\lambda) - f_T(\lambda) + c f_g(\lambda)| d\lambda. \quad (6)$$

With $f_q(\lambda)$ defined by Eqns. 3, 4 and 5, A can be written:

$$A = \int_{\lambda_{min}}^{\lambda_{max}} \left| [f_T(\lambda_{max}) - c f_g(\lambda_{max})] \left(\frac{\lambda}{\lambda_{max}} \right)^{\alpha(c, f_T, f_g)} - f_T(\lambda) + c f_g(\lambda) \right| d\lambda, \quad (7)$$

where $\alpha(c, f_T, f_g)$ is defined by Eqns. 4 and 5. Thus, one would only have to minimise A with respect to c in order to determine the maximal galactic contribution. We introduce however, an additional factor in Eqn. 7 whose purpose will be to make best use of the available data and optimise our algorithm.

2.2.1 Data Optimisation

Due to systematic effects, each Parkes optical spectrum suffers from a considerable amount of noise at the range of observed wavelengths. Although the noise may have some wavelength dependence, we assume it is constant. Given this assumption, we have used an optimal method that gives more weight to those wavelengths in a particular spectrum where the residual $|f_q(\lambda) - f_T(\lambda)|$ (see Fig. 3) is likely to be a maximum. In other words, the galaxy subtraction process will depend most sensitively on the spectral shape around the 4000Å break region. Our assumption that the noise is wavelength independent will greatly simplify our optimisation method, since otherwise, we would have to simultaneously optimise those observed spectral regions with the highest signal-to-noise.

The basis of this method simply involves convolving the integrand in Eqn. 7 with a weighting function $G(\lambda)$ that gives more weight to regions on either side of the 4000Å break within $\lambda_{min} < \lambda < \lambda_{max}$ (see Fig. 3). We choose to define $G(\lambda)$ purely from the galaxy spectrum $f_g(\lambda)$ (dashed curve in Fig. 1). This is defined as the difference (or residual) between a power-law and the galaxy spectrum within the range $\lambda_{min} < \lambda < \lambda_{max}$, containing the 4000Å break:

$$G(\lambda) = |f_{gPL}(\lambda) - f_g(\lambda)|, \quad (8)$$

where

$$f_{gPL}(\lambda) = f_g(\lambda_{max}) \left(\frac{\lambda}{\lambda_{max}} \right)^{\alpha_g}$$

and

$$\alpha_g = \frac{\ln [f_g(\lambda_{min})/f_g(\lambda_{max})]}{\ln [\lambda_{min}/\lambda_{max}]}$$

The function $G(\lambda)$ will peak at wavelengths on either side of the 4000Å break. Thus, by convolving $G(\lambda)$ with Eqn. 7, relatively more weight will be given to spectral data at these wavelengths, where our algorithm mostly sensitively depends.

Thus, the function to minimise can now be written:

$$A = \int_{\lambda_{min}}^{\lambda_{max}} \left[f_T(\lambda_{max}) - c f_g(\lambda_{max}) \right] \left(\frac{\lambda}{\lambda_{max}} \right)^{\alpha(c, f_T, f_g)} - f_T(\lambda) + c f_g(\lambda) \Big| G(\lambda) d\lambda, \quad (9)$$

where $G(\lambda)$ is defined by Eqn. 8. Our aim is to determine the value of c for a particular source spectrum $f_T(\lambda)$ such that A is a minimum. In Fig. 4, we show examples of the figure of merit function A (Eqn. 9) as a function of the parameter c for two sources whose spectra are shown in Fig. 5. If the weighting factor $G(\lambda)$ in Eqn. 9 is neglected, we find that the values of c at which A is a minimum decrease by up to 5% in most sources where the break feature appears relatively weak or absent. In sources with strong 4000Å breaks, there is no significant difference. Given the value of c that minimises A , the fractional galaxy contribution at some wavelength can now be computed using Eqn. 2.

2.3 Error Determination

In spectra where the galaxy contribution is relatively weak, an upper limit on its contribution at some appropriate level of significance would be required. In order to do so, both random and systematic errors need to be investigated. The magnitude of these two types of errors are estimated and compared in section 4.2. Here, we briefly outline the method in their determination.

2.3.1 Random (Statistical) Errors

The random error at some confidence level in the galaxy contribution is estimated by computing the value of c corresponding to the statistical error in A (Eqn. 9). Since Eqn. 9 is actually a discrete sum over wavelength bins λ_i , from λ_{min} to λ_{max} , the statistical error is determined by adding the error for each individual bin in quadrature, so that

$$\sigma(A) = \sqrt{\sum_{\lambda_i=\lambda_{min}}^{\lambda_{max}} \sigma_i^2(I)}, \quad (10)$$

where $\sigma_i(I)$ is the error in the integrand I of Eqn. 9 for bin λ_i . $\sigma_i(I)$ will depend only on uncertainties in the measured source fluxes $f_T(\lambda_{max})$ and $f_T(\lambda_{min})$ in Eqn. 9. As shall be discussed in section 3.1, these fluxes are estimated by calculating the median continuum flux in wavelength bins centered on λ_{max} and λ_{min} . We estimate the corresponding uncertainties by computing the rms deviation from the mean spectral flux in these wavelength bins.

2.3.2 Systematic Errors

Our definition of the underlying quasar continuum $f_q(\lambda)$, in each source only requires that it be smooth and contain no breaks. This implies that the shape of $f_q(\lambda)$ is somewhat arbitrary and thus it is possible that our quantitative measures of the galaxy contribution may strongly depend on its assumption in our algorithm. The uncertainty introduced by this possible systematic effect will be investigated.

All our calculations assume that $f_q(\lambda)$ is a power-law (ie. Eqn. 3), since the continua of optical quasar spectra are well represented by $f_\nu \propto \nu^{-\alpha}$ where $\alpha \sim 0.2 - 0.3$ (Francis 1996). To investigate the effects of assuming a different form for $f_q(\lambda)$ however, we also apply our algorithm by assuming for simplicity that $f_q(\lambda)$ is a straight line joining λ_{min} and λ_{max} in Fig. 3. This is parameterised as follows:

$$f_q(\lambda)_{line} = \frac{[f_q(\lambda_{max}) - f_q(\lambda_{min})]}{\lambda_{max} - \lambda_{min}} (\lambda - \lambda_{max}) + f_q(\lambda_{max}), \quad (11)$$

where $f_q(\lambda_{min})$ and $f_q(\lambda_{max})$ are defined by Eqn. 5. A comparison in the fractional galaxy contributions resulting from our use of a power-law (Eqn. 3) and a straight line (Eqn. 11) for $f_q(\lambda)$ in our algorithm, will enable us to estimate the magnitude of this systematic effect. Results are presented in section 4.2. Other possible sources of systematic error are also discussed in this section.

2.4 Summary

To summarise, we have presented in this section a method to determine the relative galaxy contribution in each Parkes

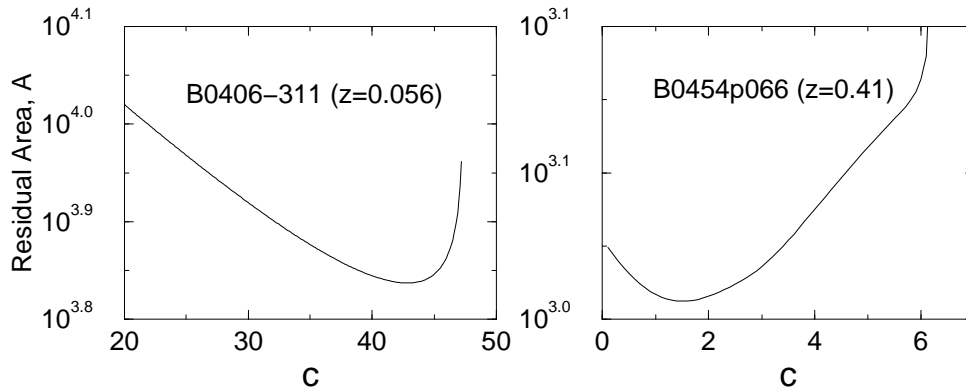


Figure 4. Examples of our figure of merit function A (defined by Eqn. 9) as a function of the parameter c . Source spectra are shown in Fig. 5.

source in a robust way. Our algorithm requires the following two input assumptions: First, an elliptical optical SED, $f_g(\lambda)$, defining the shape of the characteristic 4000\AA break. This we assume is a model from Bruzual & Charlot (1993) (see Fig. 1). Second, we require a spectral shape defining the underlying quasar spectrum $f_q(\lambda)$. Unless otherwise specified, all our calculations shall assume a power-law for $f_q(\lambda)$.

With the only requirement that $f_q(\lambda)$ be smooth and contain no breaks, the “suspected” 4000\AA break in each source spectrum $f_T(\lambda)$, is subtracted until the residual between $f_q(\lambda)$ and galaxy subtracted source spectrum is a minimum. The galaxy contribution is estimated from the amount of galaxy, $f_g(\lambda)$ subtracted. To apply this procedure in a self-consistent manner, we have defined a figure of merit given by Eqn. 9. This is minimised with respect to the parameter c from which the fractional galaxy contribution can be easily computed using Eqn. 2.

3 DATA AND INPUT PARAMETERS

Out of the 323 sources in the Drinkwater et al. (1997) sample, we have optical spectra for 194 or 60% of the sample. Some of these are from the compilation of Wilkes et al. (1983) and others are from recent observations on the AAT and ANU 2.3m (see Drinkwater et al. 1997). For these latter observations (65 sources), the spectra cover the observed wavelength range: $3200\text{\AA} \lesssim \lambda \lesssim 10000\text{\AA}$ with a resolution of $\sim 5\text{\AA}$ in the blue and $\sim 20\text{\AA}$ in the red ($\gtrsim 5200\text{\AA}$). Other spectra have typically a mean resolution $\sim 10\text{\AA}$ and cover the range: $3200\text{\AA} \lesssim \lambda \lesssim 8000\text{\AA}$.

3.1 Applying the Algorithm

Before applying our algorithm, each Parkes optical spectrum is redshifted to its rest frame. We then define the fixed rest frame wavelengths λ_{min} and λ_{max} within which the suspected 4000\AA break and our figure of merit (Eqn. 9) is defined (see Fig. 3). This wavelength region is chosen using the following criteria: first, the highest redshift sources will

have the rest wavelength λ_{max} redshifted out of the observational wavelength range of the spectra. These sources will not be able to be used in our algorithm. We therefore need to choose λ_{max} such that the number of sources in which our algorithm can be applied is not significantly reduced. Second, we need a wavelength range $\lambda_{min} < \lambda < \lambda_{max}$ that makes ‘optimal’ use of the shape of the 4000\AA break region defining our figure of merit A (the residual area in Fig. 3). In other words, we need to ensure that this region is unambiguously defined and clearly represented in each source spectrum. As a compromise, we assume $\lambda_{min} = 3500\text{\AA}$ and $\lambda_{max} = 5080\text{\AA}$ in every source.

Relative measures of the fluxes: $f_T(\lambda_{min,max})$ and $f_g(\lambda_{min,max})$ in the source and galaxy rest frame spectra respectively (see Eqn. 9), are determined as follows. We first define wavelength bins of width $\sim 200\text{\AA}$ and $\sim 400\text{\AA}$ centered on λ_{min} and λ_{max} respectively, and then calculate the median *continuum* flux in each bin. The wavelength regions defining these bins however may contain absorption and emission lines. Such lines are likely to bias our estimates of the continuum level in these regions. From the bin widths defined above, the rest wavelength regions of interest are: $3400\text{\AA} < \lambda < 3600\text{\AA}$ and $4880\text{\AA} < \lambda < 5280\text{\AA}$. From the available source spectra, we find that no lines are likely to contaminate the short wavelength bin. For the long wavelength bin however, we find that the emission line doublet [OIII] $\lambda\lambda 4959, 5007$ and a weak absorption feature at $\sim 5170\text{\AA}$ (possibly from MgI) are strong contaminants. To avoid significant contamination, our algorithm excludes regions of width 10\AA centered on these lines.

Given the definitions above, the rest wavelength range required by our algorithm will be $3400\text{\AA} \lesssim \lambda_{rest} \lesssim 5280\text{\AA}$. With a maximum observed wavelength of $\lambda_{max}(\text{obs}) \simeq 10000\text{\AA}$ in $\sim 30\%$ of the available spectra, we find that only sources with redshifts $z \lesssim 0.9$ can be used in our algorithm. In total, we have about 53 spectra in which our algorithm can be applied.

4 RESULTS

4.1 Spectral Fits

With the input parameters from the previous section, Eqn. 9 is minimised numerically with respect to the parameter c for each spectrum. Having found the value c_{min} that minimises Eqn. 9, we can reconstruct the initial source spectrum $f_T(\lambda)$ around the 4000\AA break region within $3500\text{\AA}(\lambda_{min}) < \lambda < 5080\text{\AA}(\lambda_{max})$. This is done by superimposing the maximum amount of galaxy spectrum $c_{min}f_g(\lambda)$ generated by the algorithm, and a power-law representing the underlying “smooth” quasar spectrum $f_q(\lambda)$. From Eqns. 1 and 3, these reconstructed model spectra can be represented:

$$\begin{aligned} f_T(\lambda)_{model} &= c_{min}f_g(\lambda) + f_q(\lambda) \\ &\equiv c_{min}f_g(\lambda) + [f_T(\lambda_{max}) - c_{min}f_g(\lambda_{max})] \\ &\quad \times \left(\frac{\lambda}{\lambda_{max}}\right)^{\alpha(c_{min}, f_T, f_g)}. \end{aligned} \quad (12)$$

A visual comparison between these model and observed spectra in the range $\lambda_{min} < \lambda < \lambda_{max}$ will allow us to investigate the accuracy of our algorithm in reproducing the observed spectra around the 4000\AA break region. Reconstructed spectra $f_T(\lambda)_{model}$ are compared with the observed spectra, $f_T(\lambda)$, for a number of sources in Fig. 5. On each spectrum, we also show our power-law fit $f_q(\lambda)$. Since the power-law spectral index for $f_q(\lambda)$ is defined purely within $\lambda_{min} < \lambda < \lambda_{max}$ (as required by our algorithm; see Eqns 3 and 4), a model spectrum will attempt to accurately reproduce that observed region which falls in this wavelength range only. As expected, observed spectra showing strong 4000\AA breaks with SEDs similar to that given in Fig. 1 are reproduced very accurately about the break region.

In a majority of observed spectra where no significantly strong breaks are discernable to the human eye however, our algorithm nevertheless attempts to fit for a break. Unbiased estimates of the galaxy contribution using the relative sizes of these breaks, however weak, are presented in section 4.3.

4.2 Systematic versus Random Errors

As discussed in section 2.3, a possible source of systematic uncertainty is in our assumption of the shape of the underlying smooth quasar continuum $f_q(\lambda)$. To explore this, we compare the relative galaxy contribution obtained by assuming first, a power-law (PL) (Eqn. 3) for $f_q(\lambda)$ and second, a straight line (L) (Eqn. 11). Using our algorithm and these two definitions for $f_q(\lambda)$, we have computed the fractional galaxy contribution at 5000\AA (rest frame). Results are shown in Fig. 6.

At first glance, estimates for the galaxy fraction using the power-law and straight line for $f_q(\lambda)$ agree very well. There is relatively little scatter about the diagonal line defining the equality $\text{frac}_L = \text{frac}_{PL}$, except for a distinct population with $\text{frac}_L < \text{frac}_{PL}$. No distinguishing feature in the optical spectra of this latter class is immediately apparent. It is likely that a power-law (rather than a straight line) within $\lambda_{min} < \lambda < \lambda_{max}$ for these sources provides a better representation of our figure of merit A in Fig. 3. We quantify the systematic error from the RMS scatter in the difference: $\delta = \text{frac}_L - \text{frac}_{PL}$, which we denote by $\sigma(\delta)$. For this systematic effect, we therefore estimate a 1σ uncertainty in the galaxy fraction at 5000\AA of at most $\sigma_{frac} \simeq 0.02$.

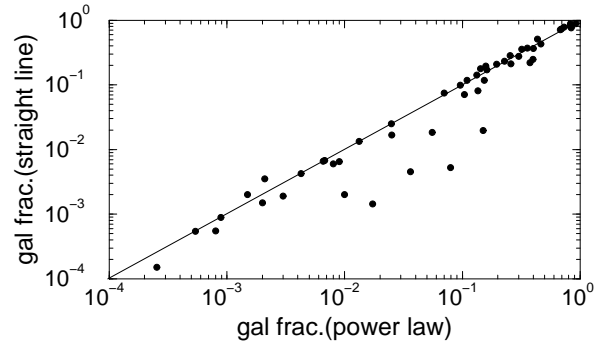


Figure 6. Fractional galaxy contribution at 5000\AA (rest frame) assuming a straight line for $f_q(\lambda)$ (vertical axis) and a power-law (horizontal axis). The diagonal line is the line of equality. (see section 4.2).

Another possible source of systematic error is in our selection of the wavelengths λ_{max} and λ_{min} , within which the suspected 4000\AA break and our figure of merit (Eqn. 9) is defined (see Fig. 3). As discussed in section 3.1, the values $\lambda_{min} = 3500\text{\AA}$ and $\lambda_{max} = 5080\text{\AA}$ were chosen as a compromise between: first, to maximise the number of sources in which the 4000\AA break remains within the observed wavelength after redshifting, and second, to make optimal use of the break region. What are the effects on the galaxy fraction if a different wavelength range were assumed?

To explore this, we choose to vary λ_{max} alone. Due to the relatively small wavelength range at $\lambda < 4000\text{\AA}$ available in the galaxy spectrum (Fig. 1), we are not as flexible in varying λ_{min} . We therefore keep λ_{min} fixed at 3500\AA . Assuming the same bin widths (200\AA and 400\AA) centered on λ_{min} and λ_{max} , and the PL definition for $f_q(\lambda)$, we have computed galaxy fractions at 5000\AA with $\lambda_{max} = 5500\text{\AA}$, and $\lambda_{max} = 6500\text{\AA}$. Combined with our estimates using $\lambda_{max} = 5080\text{\AA}$, we find that changing λ_{max} makes negligible difference in the galaxy fraction. The fractions differ by no more than 1%.

We now compare these systematic uncertainties with estimates of the random errors. Fig. 7 shows the distribution of random errors in the fractional galactic contribution at 5000\AA as determined from our algorithm (see section 2.3). The range in random errors is significantly broad, with a majority of values exceeding our maximum 1σ systematic uncertainty of 0.02 deduced from Fig. 6. In the remaining sections, we therefore quote all uncertainties in the relative galaxy contribution as purely statistical, based on random errors alone.

4.3 Galactic Contribution to the Observed Optical-Near IR Continuum.

Using our algorithm, we have computed the fractional galaxy contribution in the individual bandpasses B_J ($\lambda \simeq 4400\text{\AA}$) and K ($\lambda \simeq 2.2\mu\text{m}$), expected in an observer’s frame for each source. We estimate these using Eqn. 2 where fluxes are approximated by computing the median spectral flux at the central wavelength of each bandpass. Since our observed

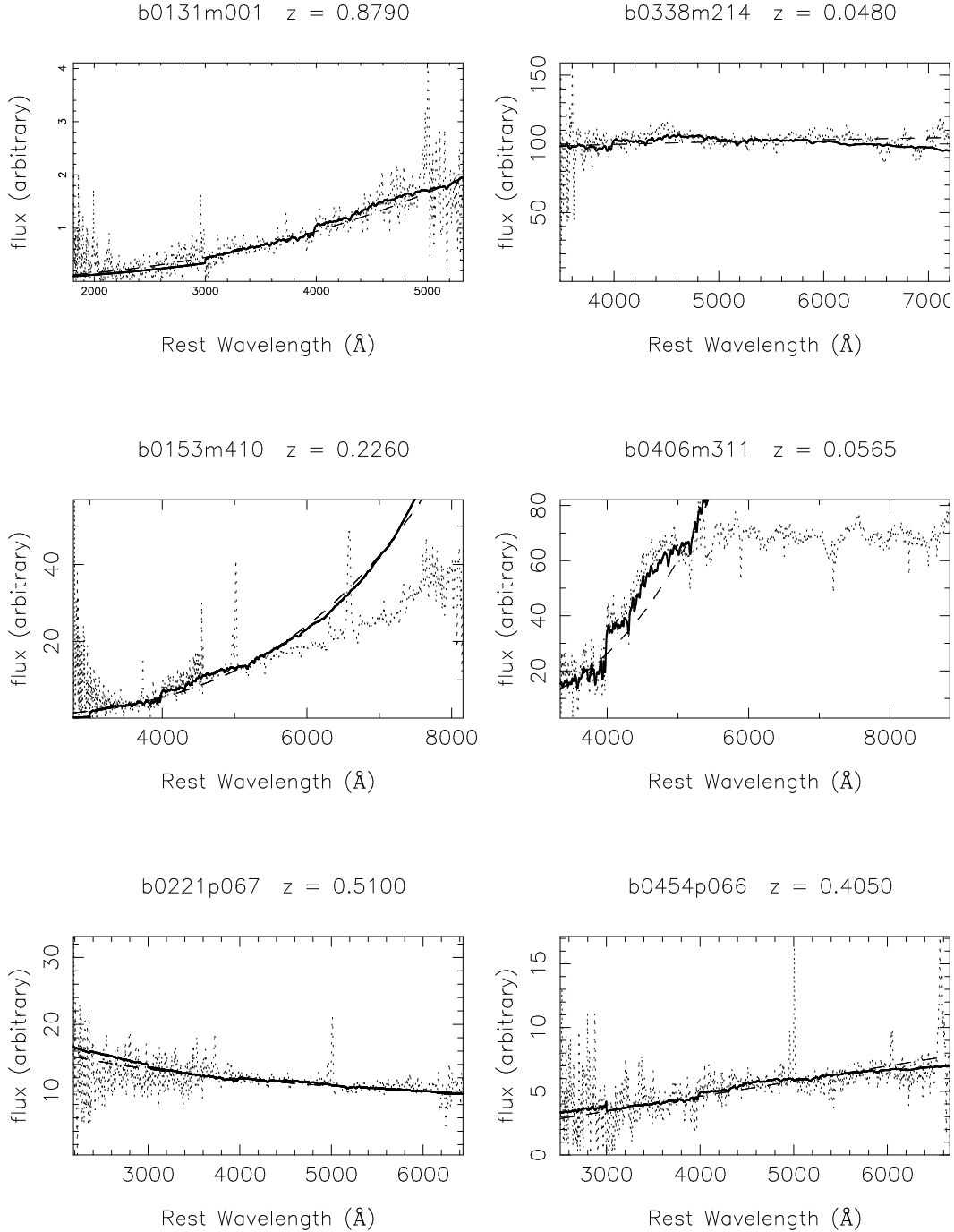


Figure 5. Observed rest frame spectra (dotted) for a number of sources in the Parkes sample. Also shown are reconstructed model spectra (solid) as defined by Eqn. 12 and power-law fits representing the underlying quasar continuum (dashed). Since this quasar spectrum is purely defined within the range $3500\text{\AA}(\lambda_{min}) < \lambda < 5080\text{\AA}(\lambda_{max})$, the model spectra are only effective in reproducing those regions observed within this wavelength range.

spectra do not extend to near-IR wavelengths, we estimate the observed spectral flux in K using our observed $B_J - K$ colours and extrapolate from the spectral flux corresponding to B_J . Unfortunately, not all of the 53 sources used in our algorithm have a measured K magnitude and hence $B_J - K$ colour. Of these sources, exactly 34 have known K magnitudes.

The distributions in galaxy fractions in B_J and K are

shown in Figs. 8a and b respectively. Sources with mean galaxy fractions $\lesssim 5\%$ are replaced by their 3σ upper limits (dashed histograms). The distributions in Figs. 8a and b appear very similar, except however for a greater number of sources with galaxy contributions $> 70\%$ in the K -band. These are all low redshift sources with strong 4000\AA breaks in their spectra. Their light is expected to be dominated by evolved stellar populations, and hence strongest in K . We

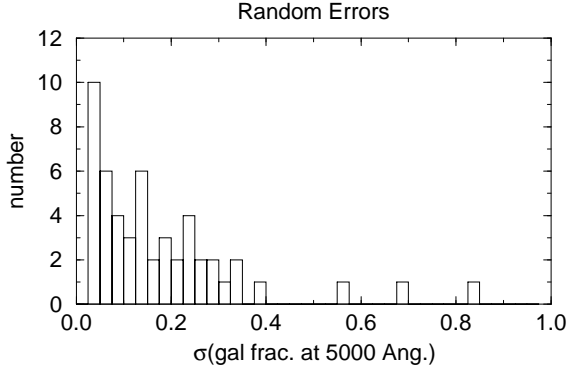


Figure 7. Distribution of 1σ random errors in the fractional galaxy contribution at 5000\AA (rest frame) for Parkes sources. (see section 4.2).

must also note that the B_J magnitudes used to estimate the K spectral fluxes via $B_J - K$ colours are only accurate to ~ 1 mag (Drinkwater et al. 1997). This photometric uncertainty is likely to contribute significant scatter in our estimates of the K galaxy fraction in Fig. 8b.

We have divided the K -band identifications into two populations: those which show extended (resolved) structure, and those which remain unresolved. The galaxy fraction in K for these two populations is shown as a function of z in Fig. 9. Open symbols represent resolved sources, and filled symbols, unresolved sources. As expected, those sources exhibiting resolved structure are also those which show large galaxy fractions and are at relatively low redshifts.

We now investigate whether emission from the host galaxies of Parkes quasars can significantly contribute to their observed $B_J - K$ colours. We do this by computing the $B_J - K$ colour of the hypothesised underlying “quasar”, $(B_J - K)_q$, we would expect if contribution from the host galaxy was absent in each source. If the observed colours were entirely due to galactic emission, then we expect the distribution in $(B_J - K)_q$ to show a relatively small scatter, i.e. similar to that observed for optically-selected quasars where typically $(B_J - K)_q \simeq 2.5$.

The colour of an underlying quasar, $(B_J - K)_q$, can be written in terms of the observed colour $(B_J - K)_{obs}$ and the galaxy fractional contributions $F_{gal}(B_J)$ and $F_{gal}(K)$ as follows:

$$(B_J - K)_q = (B_J - K)_{obs} + 2.5 \log \left[\frac{1 - F_{gal}(K)}{1 - F_{gal}(B_J)} \right]. \quad (13)$$

$(B_J - K)_q$ is plotted against $(B_J - K)_{obs}$ in Fig. 10a. As can be seen, the scatter in galaxy subtracted colours, $(B_J - K)_q$, remains and is extremely similar to that of the observed colour distribution. We quantify the galaxy contribution to the observed $B_J - K$ colours (in magnitudes) in Fig. 10b. From Figs. 10a and b, we conclude that the observed spread in colours cannot be due to emission from the host galaxies of Parkes quasars. An independent mechanism must be involved.

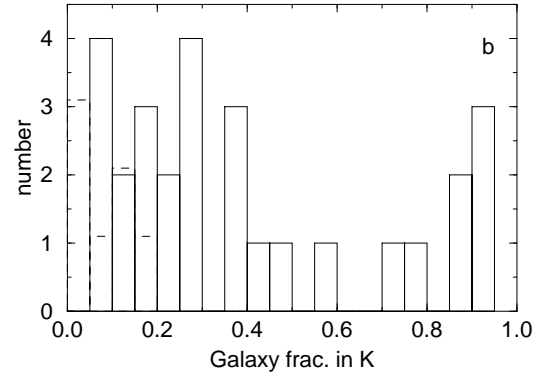
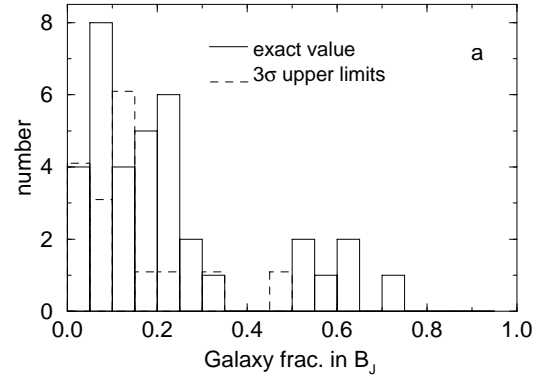


Figure 8. (a) Distribution in fractional galaxy contributions in B_J and (b) K for $z < 1$. Dashed portions represent 3σ upper limits, (see section 4.3).

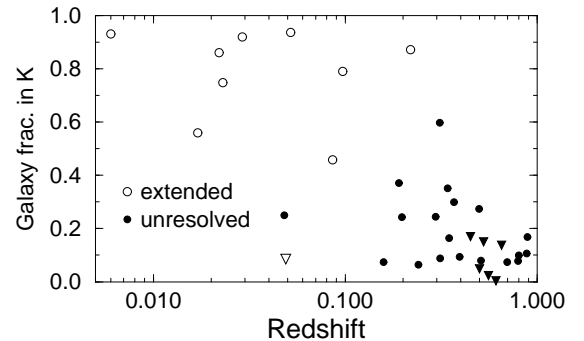


Figure 9. Fractional galaxy contribution in K as a function of redshift for resolved sources (extended on K and B_J images; open symbols) and unresolved sources (closed symbols). Triangles represent 3σ upper limits on the galaxy fraction.

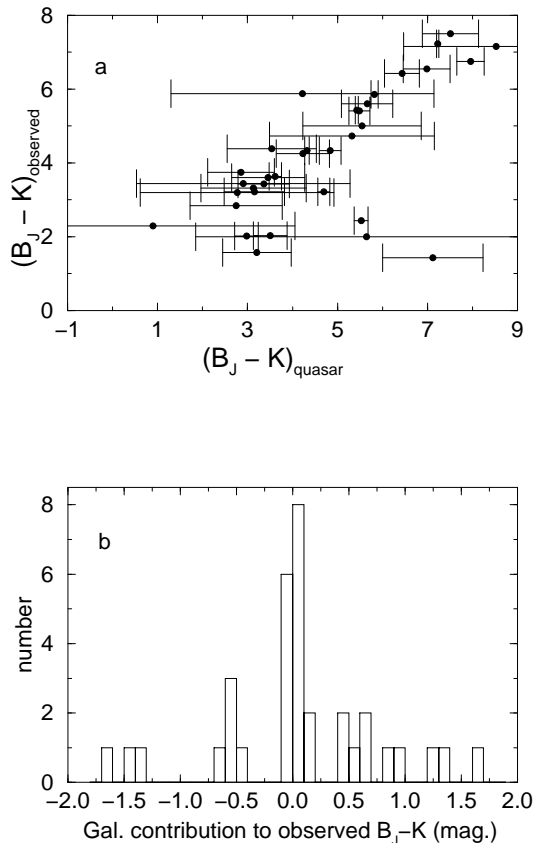


Figure 10. (a) Observed $B_J - K$ colour vs. colour of the underlying quasar (i.e. resulting galaxy subtracted colour: $(B_J - K)_q$). Error bars correspond to 1σ significance. (b) Distribution in galaxy contribution to observed $B_J - K$ colours in magnitudes.

5 A TEST FOR THE UNIFIED MODEL

Studies of the host galaxy properties of BL-Lacs and radio-quasars can be used as a test of the unified scheme for radio-loud AGN. Motivated by the canonical axisymmetric model for AGN, the basis of this scheme is that the appearance of an extragalactic radio source is primarily determined by viewing geometry. Extended FRI and FRII-type radio galaxies are believed to represent the parent (misaligned) populations of the more compact BL-Lacs and radio quasars respectively (Urry & Padovani 1995 and references therein). If classification is purely based on orientation, then intrinsic properties such as host galaxy luminosity should be approximately uniform throughout. In this section, we shall test this hypothesis.

Studies have shown that for quasars and FRII radio galaxies at redshifts $z \lesssim 0.3$, the situation is not entirely clear. From comparisons of their mean host galaxy luminosities, some studies have shown that FRII hosts are fainter by ~ 0.5 -1 mag. (Smith & Heckman 1989), while others have concluded that they are comparable (eg. Taylor et al. 1996). The main difficulty in these studies was finding sufficiently large samples of radio galaxies and quasars matched both in radio power and redshift. There is strong observational

evidence however that the low redshift BL-Lacs reside in giant ellipticals with mean optical luminosities and de Vaucouleurs $r^{1/4}$ law profiles similar to those in FRIs (Ulrich 1988; Stichel et al. 1993). Very little is known about the host galaxies of compact radio sources at higher redshifts. Using our algorithm however, we can get estimates of host galaxy K magnitudes for sources up to $z \sim 1$.

We can predict the host galaxy K magnitudes of Parkes sources directly from our estimates of the fractional galaxy contribution in the K -band, $F_{gal}(K)$ (see section 4.3). The host galaxy magnitude in an observer’s frame can be written:

$$K_{gal} = K_{source} - 2.5 \log [F_{gal}(K)], \quad (14)$$

where K_{source} is the observed K magnitude of the source. As discussed in section 4.3, $F_{gal}(K)$ is determined from the median spectral flux at $\lambda \simeq 2.2\mu\text{m}$ (Eqn. 2), which we estimate using the observed spectral flux at $\lambda \simeq 4400\text{\AA}$ and $B_J - K$ colour.

Estimates of K_{gal} as a function of redshift are shown in Fig. 11. For comparison, we also show the range observed for radio galaxies (shaded region) as determined from a number of independent studies (McCarthy 1993). Within our quoted uncertainties, there appears to be no significant difference in the mean host galaxy magnitude of “compact” Parkes sources and extended radio galaxies at the redshifts indicated. The compact sources however appear to show a larger scatter in K_{gal} at some redshift. Since the K_{gal} values were determined from non-contemporaneous measures of observed B_J spectral fluxes and $B_J - K$ colours, this may be attributed to variability in the underlying AGN. We are unable at present to quantify this uncertainty. From Fig. 11, we conclude that the host galaxy luminosities of these two classes of radio source is consistent with that required by the unified model.

6 DISCUSSION

Our results of section 4.3 clearly show that galactic emission is unlikely to fully explain the dispersion in $B_J - K$ colours observed. This conclusion is only valid however for sources at redshifts $z \lesssim 0.9$. At higher redshifts, the 4000\AA break feature on which our algorithm is based is redshifted out of our observational wavelength range. Taking into account our completeness in spectral data (section 3), only 53 of the 323 sources in the Drinkwater et al. (1997) sample have been analysed using our algorithm. Since we are limited to redshifts $z \lesssim 0.9$, it is possible that we are biased towards detecting relatively large galaxy contributions. Our results may thus not be representative for the whole sample of Parkes quasars.

We have two strong pieces of observational evidence that supports a minimal galaxy contribution from the high redshift Parkes sources: First, all sources with $z \gtrsim 0.5$ appear very compact in K (eg. Fig. 9), and exhibit broad-line equivalent widths typical of those observed in optically-selected quasars. Second, significantly high levels of linear polarisation ($\gtrsim 5\%$) have been observed in the near-IR in several sources at $z \gtrsim 1$ (see Masci 1997). This strongly indicates that the emission is dominated by a non-thermal mechanism. It is important to note however that the number of sources in which a polarisation has been searched for is too low to

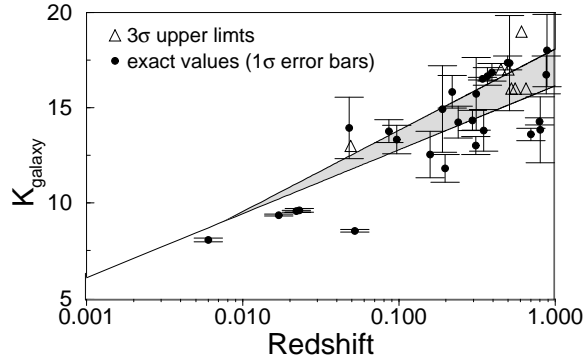


Figure 11. Host galaxy K magnitude as a function of redshift for Parkes sources (symbols) and the range observed for radio galaxies (shaded region; McCarthy 1993).

draw any reasonable conclusion. Further polarimetric studies of preferably the reddest quasars are necessary to assess the importance of a host galaxy component.

The next significant step in improving the algorithm presented here for determining the galaxy contribution would be to completely discard our assumption of a power-law for the shape of the underlying quasar spectrum. Although a simple power-law is a good overall representation for the *continuum* around $\lambda \simeq 4000\text{\AA}$, generic quasar spectra also include a complex blend of emission line features superimposed on the continuum about this region. As seen in most compilations of composite QSO spectra (eg. Francis et al. 1991), wavelengths shortwards of 3700\AA are contaminated by a Balmer continuum, where emission from the convergence of high order Balmer lines can introduce a steep rise in this part of the spectrum. Furthermore there is also a complex blend of FeII emission setting in at these wavelengths. These considerations therefore invalidate our assumption of a pure power-law for the “smooth” quasar spectrum. Nonetheless, it is likely that the omission of these additional intrinsic features at $\lambda \lesssim 4000\text{\AA}$ will have led us to overestimate the galaxy contribution on average.

7 CONCLUSIONS

This paper has explored whether emission from the host galaxies of Parkes quasars can significantly contribute to the relatively large spread in $B_J - K$ colours observed. If the hosts are classical giant ellipticals and their flux strongly contributes, then this would be expected since elliptical colours are known to be quite red in $B - K$ to $z \sim 2$.

We have devised an algorithm that measures the relative galaxy contribution in each source in an unbiased way using the characteristic 4000\AA break feature of elliptical galaxy SEDs. The basis of the algorithm involves subtracting a generic elliptical SED from each source spectrum until the 4000\AA break feature disappears and what is left is a “smooth” spectrum containing no breaks. This “smooth” spectrum we refer to as the underlying quasar spectrum. The only requirement by our algorithm is that this remaining spectrum be smooth. The galactic contribution, relative

to the total light at any wavelength is estimated from the amount of galaxy subtracted.

The main conclusions are:

1. For $z \lesssim 0.9$, (for which the 4000\AA feature remains observable in our spectra), we find broad and almost bimodal distributions in the relative galaxy fraction in B_J and K . Most sources ($\gtrsim 70\%$) have galaxy fractions < 0.3 at the 3σ level in both B_J and K . The remainder have large galaxy contributions and are predominately low redshift galaxies with strong 4000\AA breaks. All of these latter sources are spatially extended and resolved on B_J and K -band images. In particular, there is a clear distinction in the strength of the 4000\AA break for resolved and unresolved sources.

2. Using these estimates, we find that the mean K -band magnitude of the host galaxies of flat spectrum radio quasars is consistent with that of extended radio galaxies at $z \lesssim 0.9$. This is consistent with the unified model for radio-loud AGN.

3. By subtracting the galaxy contribution in each band-pass from the observed $B_J - K$ colours of Parkes sources, we find that at predominately the 2σ confidence level, the relatively large spread in colours still remains. We conclude that in a majority of cases, the relatively red colours must be due to a mechanism other than that contributed by a “red” stellar component.

8 ACKNOWLEDGMENTS

FJM acknowledges support from an APRA Scholarship, and RLW from an ARC research grant.

REFERENCES

- Bahcall J.N., Kirhakos S., Saxe D.H., Schneider, D.P., 1995, *ApJ*, 479, 642
- Benn C.R., Vigotti M., Carballo R., Gonzalez-Serrano J.I., Sánchez S.F., 1998, *MNRAS*, in press, astro-ph/9710301
- Bruzual G., Charlot S., 1993, *ApJ*, 405, 538
- Drinkwater M.J., Webster R.L., Francis P.J., Condon J.J., Ellison S.L., Jauncey D.L., Lovell J., Peterson B.A. Savage A., 1997, *MNRAS*, 284, 85
- Dunlop J.S., Peacock J.A., Savage A., Lilly S.J., Heasley J.N., Simon A.J.B., 1989, *MNRAS*, 238, 1171
- Francis P.J., Hewett P.C., Foltz C.B., Chaffee F.H., Weymann R.J., Mossis S.L., 1991, *ApJ*, 373, 465
- Francis P.J., 1996, *PASA*, 13, 212
- Guideroni B., Rocca-Volmerange B., 1987, *A&A*, 186, 1
- Hutchings J.B., Morris S.L., 1995, *AJ*, 109, 1541
- Masci F.J., 1997, PhD thesis, University of Melbourne, astro-ph/9801181
- McCarthy P.J., 1993, *ARA&A*, 31, 639
- Miller J.S., French H.B., Hawley S.A., 1978, in Wolf A.M., ed, Pittsburgh Conf. on BL-Lac Objects, Pittsburgh, p.176
- Serjeant S., Rawlings S., 1996, *Nature*, 379, 304
- Smith E.P., Heckman T.M., 1989, *ApJ*, 341, 658
- Spinrad H., Djorgovski S., 1987, in Burbidge G., ed, Proc. IAU Symp. No. 126, p.129
- Stickel M., Fried J.W., Kühr H., 1993, *A&AS*, 98, 393
- Taylor G.L., Dunlop J.S., Hughes D.H., Robson E.I., 1996, *MNRAS*, 283, 930
- Ulrich P.J., 1988, in Maraschi L., Maccacaro T., Ulrich M., eds, Conference on BL Lac Objects, Como, Italy, p.45
- Urry C.M., Padovani P., 1995, *PASP*, 107, 803

Webster R.L., Francis P.J., Peterson B.A., Drinkwater M.J.,
Masci F.J., 1995, *Nature*, 375, 469
White S.D.M., Frenk C.S., 1991, *ApJ*, 379, 52
Wilkes B.J., Wright A.E., Jauncey D.L., Peterson B.A., 1983,
PASA, 5, 2